Original Article
Food Science and Technology

ISSN 0101-2061 (Print)
ISSN 1678-457X (Online)

DOI: https://doi.org/10.1590/fst.108022

Cross-linked graphene oxide framework to enhance pervaporation separate property of waterborne polyurethane in food packaging materials

Lei SANG[1], Lu-lu YAO[2], Zhao-Jun WEI[3,4*]

Abstract

In order to improve separating aromatic/aliphatic group in adhesives or solvents of food packaging materials by pervaporation, an across linked graphene oxide (GO) framework were incorporated into waterborne polyurethane (WPU) membrane. The improved benzene solubility and expanded interlayer pathway of modified membrane have been gained based on three different reduced graphene oxide. Compared to P-phenylenediamine (PPD) and ethane-diamine (EDA) reducing agents, O-phenylenediamine (OPD) showed a relatively mild reducing ability and allowed GO to form a layer-to-layer lamella in the WPU matrix easily. When the dose of GO-OPD was 0.03%, the flux of GO-OPD/WPU membrane was 1.58 times of neat WPU or GO/WPU membranes, while the separation factor was slightly improved. The GO-OPD /WPU membrane also maintained good stability in the continuous pervaporation process of 2700 min.

Keywords: O-phenylenediamine; graphene oxide; waterborne polyurethane; pervaporation separation; packaging materials.

Practical Application: The main purpose of this study was to design and evaluate the separating ability of modified WPU membranes, based on three different reduced graphene oxide. Therefore, the results provided a natural, biodegradable, eco-friendly, and sustainable membrane to eliminate toxic aromatic solvents in food packaging materials.

1 Introduction

Some methylbenzene or xylene always be used as solvent in bag printing ink, food packaging film adhesives. These solvent residues may be converted to benzene vapor accumulation in packaging materials at high temperature, along with permeating in food, injuring hematopoietic function and destroying the nervous system subsequently. It is necessary to separate this poisonous benzene from aromatic /aliphatic hydrocarbon compound of solvent.

It is a challenge to separate the aliphatic / hydrocarbon system by molecular sieving techniques, for benzene is similar in size and polarity to cyclohexane and easily to form azeotrope mixture. Recently, some pervaporation polymer membranes have been proved to promote the penetration of benzene formally using the solution-diffusion model (Yang et al., 2020). The polar groups in polymer are conducive to interact with benzene containing P orbitals by the π-π, the effect, while other aliphatic hydrocarbons are not affected. For pervaporation technology, one material will show a higher affinity to membrane material than the other to be separated from the system, which has been successfully used for dehydration of organic solvent, removal of organic matter in water and separation of organic-organic system (Muller et al., 2020). Some polymer films such as non-toxic cellulose butyl ester (Nairat et al., 2022), polypyrrole (Ramanavičius et al., 2022), polyvinyl alcohol (Panda et al., 2022), polyethylene (Esmaeili-Faraj et al., 2021), polyester (Rostovtseva et al., 2022), polyurethane (Wu et al., 2022) are used in the membrane of separation. Water-borne polyurethane (WPU) is the only type of polymer that shows both thermos plasticity (Akram et al., 2022) and thermosetting properties in membrane materials (Liu et al., 2019), which has significant advantages in the field of pervaporation membranes.

However, the biggest challenge of organic membranes is the high swelling rate, resulting in low selectivity and low mechanical strength of membranes. To overcome these drawbacks, Water-borne polyurethane may be surface-modified with Graphene oxide (GO) by Polymerization. GO with a large ratio of vertical and aspect ratios can form a directional arrangement in the polymer matrix. The research from of Joshi (Joshi et al., 2014) shows that the effective transmission length of parallel graphene channels is L * H / d, which provides a fast and direct path for the components to be separated. However, the strong aggregation tendency and inherent inert surface of GO sheets result in the weak mechanical strength and poor chemical stability in practical application. (Jia et al., 2016). Many efforts have been done to modify GO, such as rearrangement of GO 's oxygen-containing hydrophobic group (Xu et al., 2017), or applying reducing agent containing benzene rings to form rigid structures to expand GO interlayer channels (Qian et al., 2018), or doping GO into a certain polymer matrix to prepare a modified separation membrane material with excellent performance (Chen et al.,

Received 30 Sept., 2022
Accepted 14 Nov., 2022
[1] *Department of Pharmacy, Anhui Medical College, Hefei, China*
[2] *School of Chemistry and Chemical Engineering, Hefei University of Technology, Hefei, China*
[3] *School of Food and Biological Engineering, Hefei University of Technology, Hefei, China*
[4] *School of Biological Science and Engineering, Collaborative Innovation Center for Food Production and Safety, North Minzu University, Yinchuan, China*
*Corresponding author: zjwei@hfut.edu.cn

2018; Sun et al., 2017). Furtherly, considering environmental protection, the compatibility of GO with the membrane matrix needs to be brought to the forefront. Comparing to the modify agent of –HS (Yang et al., 2018), hydrazine (Burshtein et al., 2022), $NaBH_4$ (Shen et al., 2021), hydroquinone (Sabry et al, 2022), concentrated H_2SO_4 (Kong et al., 2018), alumina powder (Wu et al., 2021), etc. Diamine has better dispersibility and gas sensitivity (Wang et al., 2020), and be expected to increase GO surface active sites, reduce polymer lattice defects and nanopores.

In order to apply GO-WU membrane in the pervaporation process of dissolution-diffusion model, a cross-linking aromatic modifier p-phenylenediamine (PPD), o-phenylenediamine (OPD) were used to prepare reduced GO (PPD-GO, OPD-GO) respectively, and aliphatic ethylenediamine (EDA)- reduced GO (EDA-GO) was used as reference sample. The key to the application of graphene oxide modified waterborne polyurethane (GO/WPU) membrane was the accurate regulation of layer spacing. These prepared GO and reduced GO are mixed with WPU separately to fabricate assembled membrane, aiming at expanding the diffusion performance of the system through the expansion channels of GO, and increasing the solubility by the π-π conjugation between GO and benzene.

2 Materials and methods

2.1 Raw materials

Graphite powder (99%) concentrated H_2SO_4 (96%), H_3PO_4, HCl (53%), $KMnO_4$, ethylenediamine (AR) p-phenylenediamine (CP) o-phenylenediamine (CR)were all purchased from Sinopharm Chemical Reagent Co. Ltd. (Shanghai, China). Isophorone diisocyanate (IPDI), poly(tetra methylene glycol) (PTMG;molecular weight 2000 g/mol), and dimethylol propionicacid (DMPA) were all industrial grade and purchased from Hefei Anke Chemical Co. (Anhui, China). PTMG was dried at 120 °C in vacuo for 1 day before use, and the other chemicalswere used as received. Deionized (DI) water was laboratory self-made.

2.2 Preparation reduced Graphene oxide

Graphene oxide (GO) was synthesized by a modified Hummers method (Joshi et al., 2021) 0.1 mol/L ethylenediamine (EDA), 0.1 mol/L p-phenylenediamine (PPD), and 0.1 mol/L o-phenylenediamine (OPD) was mixed with 0.25 mg/mL GO solution at equal volume at room temperature respectively, and magnetically stir for 0.5 h. After centrifuged and washed with deionized water for several times to remove unreacted components, the filtered were dried under vacuum at 60 °C to obtain three reduced GO (rGO) powders GO–EDA, GO–OPD, GO – PPD.

2.3 Preparation modified GO/WPU membrane

GO (10 mL, 0.1 mg/mL) and the three rGO (10 mL 0.1 mg/mL) dispersions were added slowly into WPU prepolymer lotion (Sang et al., 2018) after ultrasonic for 20 minutes, followed by chain extension and emulsify stirring for 1.5 h below 10 °C, a brownish yellow emulsion with a solids content of about 20% was gained. Subsequently, the precursor emulsion formed into membrane by salivation film formation method. All the products are vacuum drying and stored in a desiccator to prevent moisture. Finally, graphene oxide-modified polyurethane membrane with doping amount of 0.03 wt% of GO or rGO were obtained, which were named as GO / WPU, GO–EDA / WPU, GO–OPD / WPU, and GO–PPD/ WPU respectively.

2.4 Charaterization

Attenuated total reflection-Fourier transform infared (ATR-FTIR) spectra of WPU membranes were recorded on an FTIR (FT-IR, PE LX10-8813, USA), x-ray photoelectron spectrometer (ESCALAB250Xi, Thermo, American) were used to characterize the change of surface functional groups. X-ray diffractometer (XRD, Rigaku Corporation D/MAX2500V, Japan) was used to characterize the microstructure of WPU membranes. The GO-WPU emulsion were dropped on a copper grid for direct transmission electron microscopy (TEM, Hitachi-H800, Japan) examination. GO-WPU membrane profile preparation by ultramicrotome (Cambridge Instruments ULTRACUTE 970114), and detected by a transmission electron microscopy (TEM) instrument (JEOL, JEM-100SX, Japan). Freeze-fractured surfaces of the samples in liquid nitrogen were examined using a field emission scanning electron microscopy (SEM) (Hitachi-SU8020, Japan). Five nanometer of Au was sputtered (Denton Desk V Sputter system) on the film surface before imaging. Atomic force micrographs (AFM) (Fastscan, Bruker, Germany) were acquired using a silicon tip on a silicon nitride cantilever in the tapping mode. Raman spectra of GO were recorded using a 532 nm laser source (HR Evolution, HORIBA JOBIN YVON, French). Pervaporation separation property were measured on for pervaporation experimental apparatus (Custom made, Suzhou Xinwang, China) The pervaporation conditions were 50 ± 3 °C, the concentration of benzene was 50wt.%, and the membrane flow rate was $25 L \cdot h^{-1}$. Flux and separation factor are respectively represented by J and α (Sang et al., 2018).

3 Results and discussion

3.1 Morphology of GO and rGO

All the samples were observed through TEM after ultrasonic dispersion in cold water below 10 °C for 20 minutes. From Figure 1a, a large sheet of transparent gauze with several micron thick and a small number of wrinkles could be observed on the surface of GO. This was the typical morphology of graphene as it adapts to the thermal fluctuations and maintain its stability (Peng et al., 2017). More wrinkles appeared on the surface of GO-OPD (Figure 1b), GO-PPD (Figure 1c) and GO-EDA (Figure 1d) samples. Hence, the various morphology of rGO was mainly reflected in the changing of roughness and accumulation state. It could be inferred that the oxygen-containing functional groups of GO would react with the $-NH_2$ of diamine, resulting in the increase structural defects and wrinkles of GO. It was also visible that the edge layer of the GO-OPD (Figure 1b) or GO-PPD (Figure 1c) were dislocation stacking, while some black agglomerates flaked in GO-EDA samples (Figure 1d), indicating GO-EDA have lost its two-dimensional structure characterized by thin and transparent morphology. The accumulation morphology of GO-EDA flakes was consistent with the poor dispersion of GO in polymer, arising from the disappearing functional oxygen-

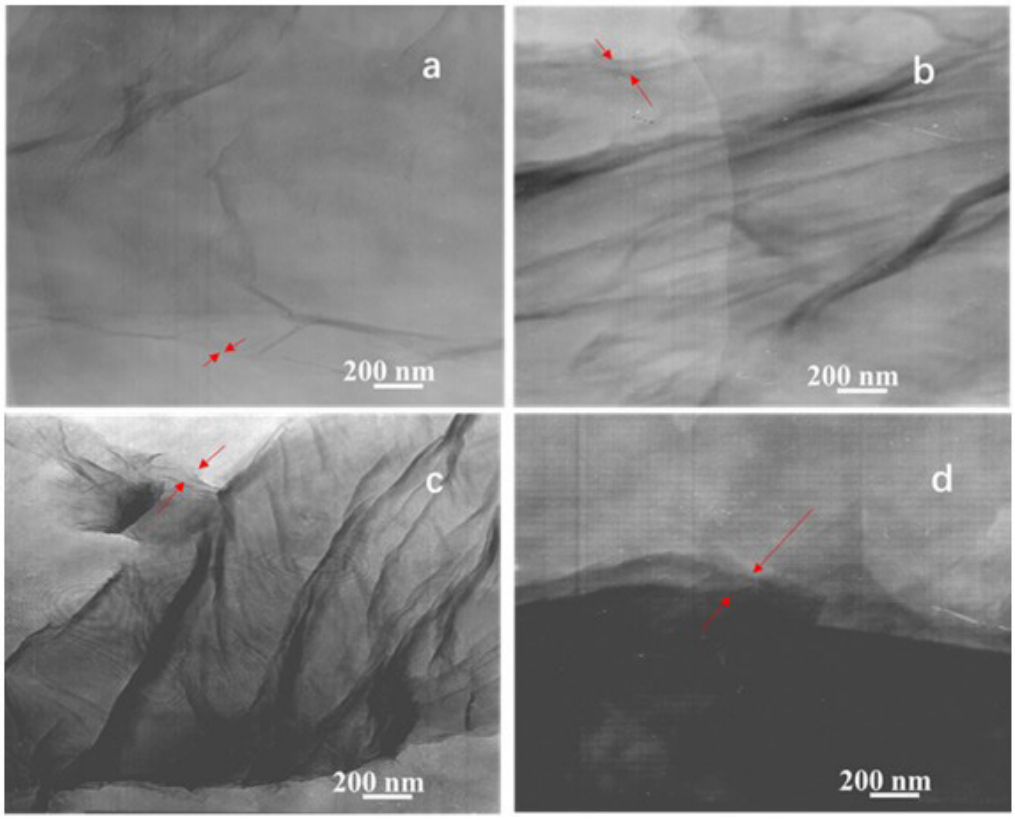

Figure 1. TEM images of different reduced graphene oxide. (a) GO; (b) GO –OPD; (c) GO-PPD; (d) GO-EDA.

containing groups at the GO edges Accordingly, the difference also illustrated the diversity ability of three reducing agents.

3.2 Chemical structure of GO and rGO

Raman spectra was shown in Figure 2, with verifying the main changes of carbon layer structure. The G peak near 1580 cm^{-1} was a characteristic peak of the Carbon sp^2 structure, reflecting the symmetry and degree of crystallinity. And the D peak near 1350 cm^{-1} was a characteristic peak of the defect peak, reflecting the disorder of the graphene sheet (Peng et al., 2017). The calculation results were listed in Table 1. Compared with the G peak position of GO (1598 cm^{-1}), GO-OPD (1578 cm^{-1}), GO-PPD (1571 cm^{-1}), and GO-EDA (1580 cm^{-1}) move to a low wavenumber direction. From this, it may be deduced that the rGO has isolated double bonds, which resonated at a higher frequency than the G band of GO, but near the G band of graphite (1581 cm^{-1}) (Viveka et al., 2022), which corresponds to the restoration of a defective hexagonal network of carbon atoms.

The I_D / I_G values and the sp^2 hybrid region size of Cabon was calculated according to the Formula 1 of the literature (Lada, 2022).

$$\mathrm{Lanm} = 2.4\times10^{-10}\lambda^4\left(\frac{I_D}{I_G}\right)^{-1} \quad (1)$$

La is the crystal size of the sp2 hybrid region of C, λ is the wavelength of the incident light, and ID / IG is the relative intensity ratio of the D peak and the G peak

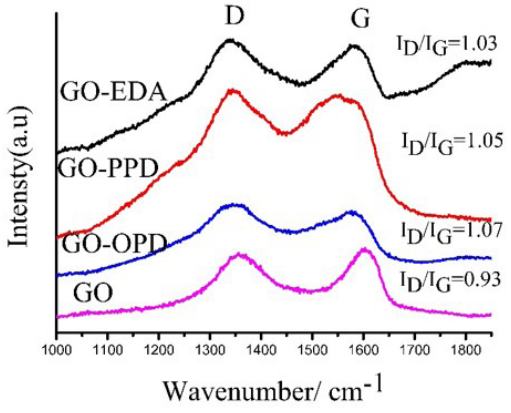

Figure 2. Raman spectra of different samples.

It can be seen that compared to the La value of GO (20.67 nm), GO-OPD (17.99 nm), GO-PPD (18.41 nm) and GO-EDA (18.66 nm) decrease significantly, meaning the reduction of the C sp^2 hybrid region to some degree. This can be explained by the presence of more structural defects on the surface after reduction (Wang et al., 2022a). Some scholars believed that the size of the sp^2 region of the newly formed graphitized C will decrease, but the number will increase after reduction (Wang et al., 2022b). In this study, the sp^3 hybrid region of C may be formed on the graphene surface due to reduction. According to the above data, the influence degree of the three modifiers on the change of C sp^2 region is arranged following the order EDA> PPD> OPD.

The infrared spectra of different reduced GO are shown in Figure 3a. In GO samples the absorption peaks at 3410 cm^{-1}, 1750 cm^{-1} and 1050 cm^{-1} were caused by the stretching vibration of –OH, C=O and C-O-C respectively, but almost disappeared in the GO-OPD, GO-PPD and GO-EDA samples. The peak of 3250 ~ 3500 cm^{-1} and 1552 cm^{-1}-1515 cm^{-1} attributed to N-H stretching vibration occurred in the rGO samples instead. This fact indicates that the GO sheets is connected together mainly by the hydrogen bonds and π-π interaction. But after modification,the interaction between rGO sheets is more than the two forces mentioned above, the bond between the oxygen-containing functional group and the amino group must to be consideration.

The changes in surface functional groups were characterized by XPS. C1s, O1s, and N1s spectra were observed at 285 eV, 533 eV, and 400 eV respectively in Figure 3b. The O/C ratio decreases in the order of GO (0.64) > GO-OPD (0.48) > GO-PPD (0.39) > GO-EDA (0.34). The conversation of oxygen-containing functional groups on the surface of GO, in corresponding to the reducing capacity of different reagents. The content of N increases in the order of GO (0) < GO-OPD (4.43%) < GO-PPD (5.11%) < GO-EDA (5.66%), reflecting the difference of the three modifiers implanted content in GO. It could be inferred that the OPD show a milder reducing ability than PPD and EDA agents, which is consistent with the Raman test result.

3.3 Chemical stucture and morphology analyses of the GO-OPD/WPU membrane

The infrared spectra of different membranes were shown in Figure 4. The main characteristic peaks of WPU are basically unchanged before and after modification, indicating GO or rGO interacts physically with WPU. The influence of OPD, PPD, and EDA on the WPU membrane are revealed in the changing of characteristic peaks at 1637 cm^{-1} (C = O ... HN hydrogen bonding C = O stretching vibration) and 1552 cm^{-1}-1515 cm^{-1} (C = O ... HN hydrogen bonding NH stretching vibration). From GO-OPD / WPU spectra, the peak at 1637 cm^{-1} disappeared. While in GO-PPD / WPU membrane, the hydrogen-bonded NH stretching vibration peak change from a broad peak to a sharp peak. And in GO-EDA / WPU membrane, the C = O hydrogen-bonded carbonyl peak moved toward the high wave. This variation indicated that hydrogen bonding between the GO and the WPU were influenced by the chemical structure of the reducing agent.

Atomic force microscopy (AFM) study (Figure 5ab) provided direct evidence for GO lamellar thickness (Alshamkhani et al., 2022). As observed in Figure 5a, the self-made GO nano-material was a large two-dimensional structure with a size of 2-7 μm and a thickness of 0.6-1.2 nm, which was close to a single or few layers. However, OPD-GO AFM spectrum (Figure 5b) basically maintained its layer-layer structure, and displayed more misaligned sheets and more thick layers.

Unfortunately, not all modifiers have a positive effect. Some modifying methods may cause a dilemma situation, because modifier agent will consume the oxygen-containing functional groups between the GO sheets, resulting in poor GO dispersibility in the polymer. Accordingly, the modifier is apt to interact with the inner -O- and -OH groups of GO instead of outside (Saini et al., 2018), which will spatially block the π-π interaction between the face-to face layers and expand the channel diameter. These two competing factors cause the complexity of the GO modify project.

Table 1. Raman Spectroscopy results of different GO powders.

Sample	D band (cm^{-1})	G band (cm^{-1})	I_D/I_G (%)	La (nm)
GO	1358	1598	0.93	20.67
GO-OPD	1342	1577	1.07	17.99
GO-PPD	1340	1571	1.05	18.41
GO-EDA	1340	1580	1.03	18.66

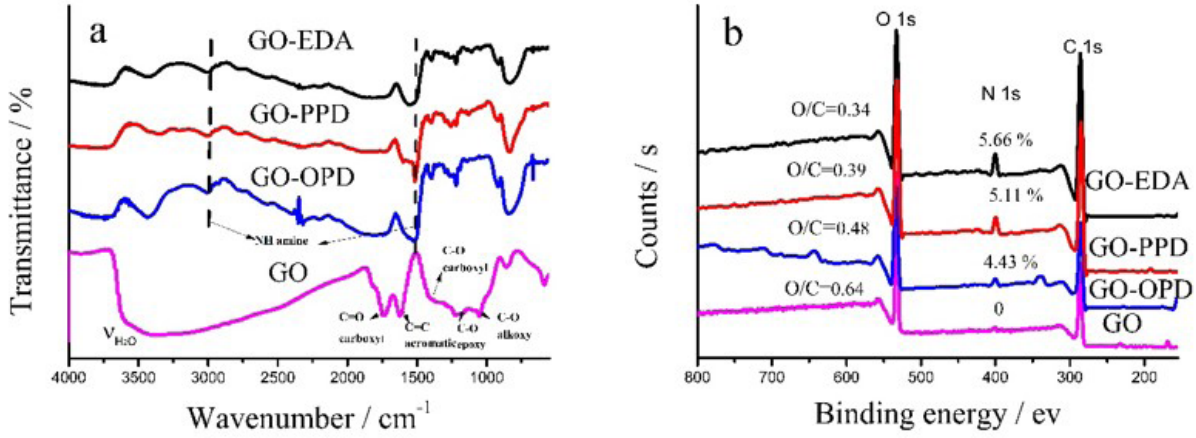

Figure 3. FTIR spectra (a) and XPS spectra (b) of different graphene oxide.

Figure 5c, d displayed the result of Ultra-thin- nano-slice TEM test, which was used to depict the morphology of rGO in WPU membranes. From GO / WPU morphology (Figure 5c), no significant agglomeration of GO could be found in aqueous polyurethane, except for inter-layer stack occur in the boundary layer. In the GO-OPD / WPU samples (Figure 5d), the surface of GO-OPD morphology was apparently darkened due to the number of stacked layers. Therefore, the gaps were visible at the edges, may be formed by stacking between layers which was further confirmed by XRD results.

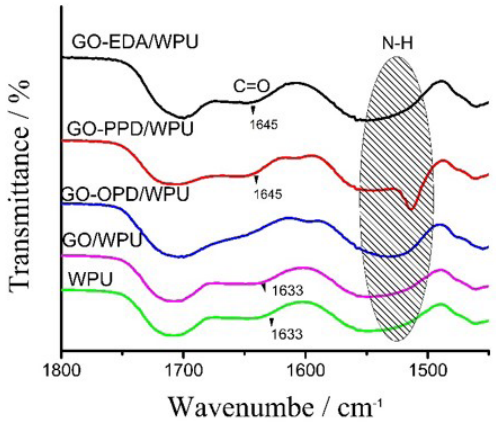

Figure 4. ATR- FTIR spectra of the different GO/WPU and GO-OPD/WPU samples.

3.4 Pervaporation performance of rGO/WPU membrane

The effect of GO on the structure of WPU membrane channels was also related to the molecular structure of the crosslinks. The cross-linking of GO by steric barrier modifiers may be divided into three cases: parallel cross-linking, vertical cross-linking, and circular cross-linking, but parallel cross-linking does not change the distance between layers (Pramoda et al., 2017). In order to investigate the effect of three reducing agents on the interlayer structure of GO, the distance d of the layer was measured by XRD. As shown in Figure 6a, there was a diffraction peak ($2\theta = 10.02°$) of typical 001 crystal plane (Joshi et al., 2014) in the GO sample, and the corresponding interlayer distance d was about 9.16 nm. In the GO-OPD samples, the diffraction peak moved to 5.96 ° (d = 14.81 nm), and graphitized diffraction peaks appeared at 19.81° (d = 4.84 nm) (Peng et al., 2017). In the GO-PPD samples, the diffraction peak below 10° became broad, with a sharp peak at 19.37°, and the corresponding interlayer distance was 4.57 nm. In the GO-EDA samples, the diffraction peak below 10° completely disappeared, only at 23.14° (d = 3.84 nm) of characteristic peaks close to graphite (23°, d = 3.86 nm) appeared. Thus, only in the GO-OPD samples, the increasing layer spacing was detected.

This process is explained by the cartoon picture of Figure 6b. There was certain distance between GO sheets, because of the existing the inner H_2O molecules adhering to GO oxygen-containing functional groups by hydrogen bonding. When H_2O

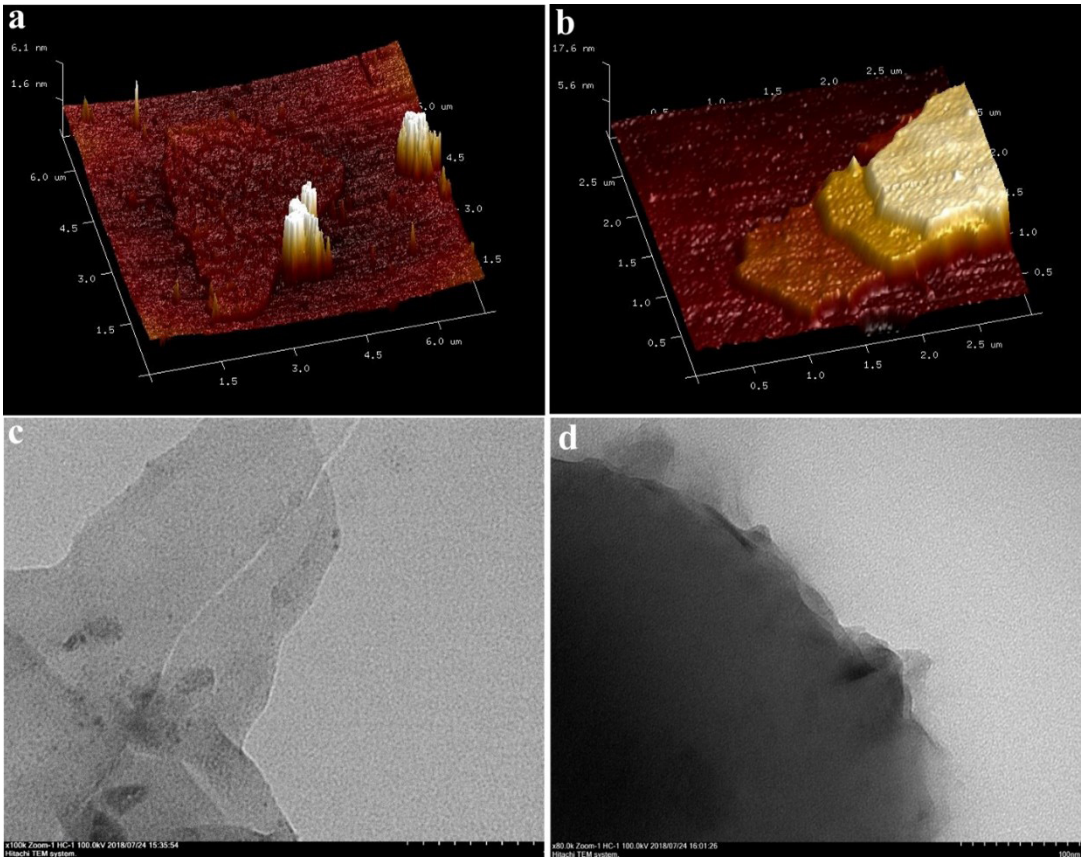

Figure 5. Microtopography of different GO/WPU and GO-OPD/WPU samples (a-b display AFM spectrum, c-d is the result of Ultra-thin-nano-slice TEM test).

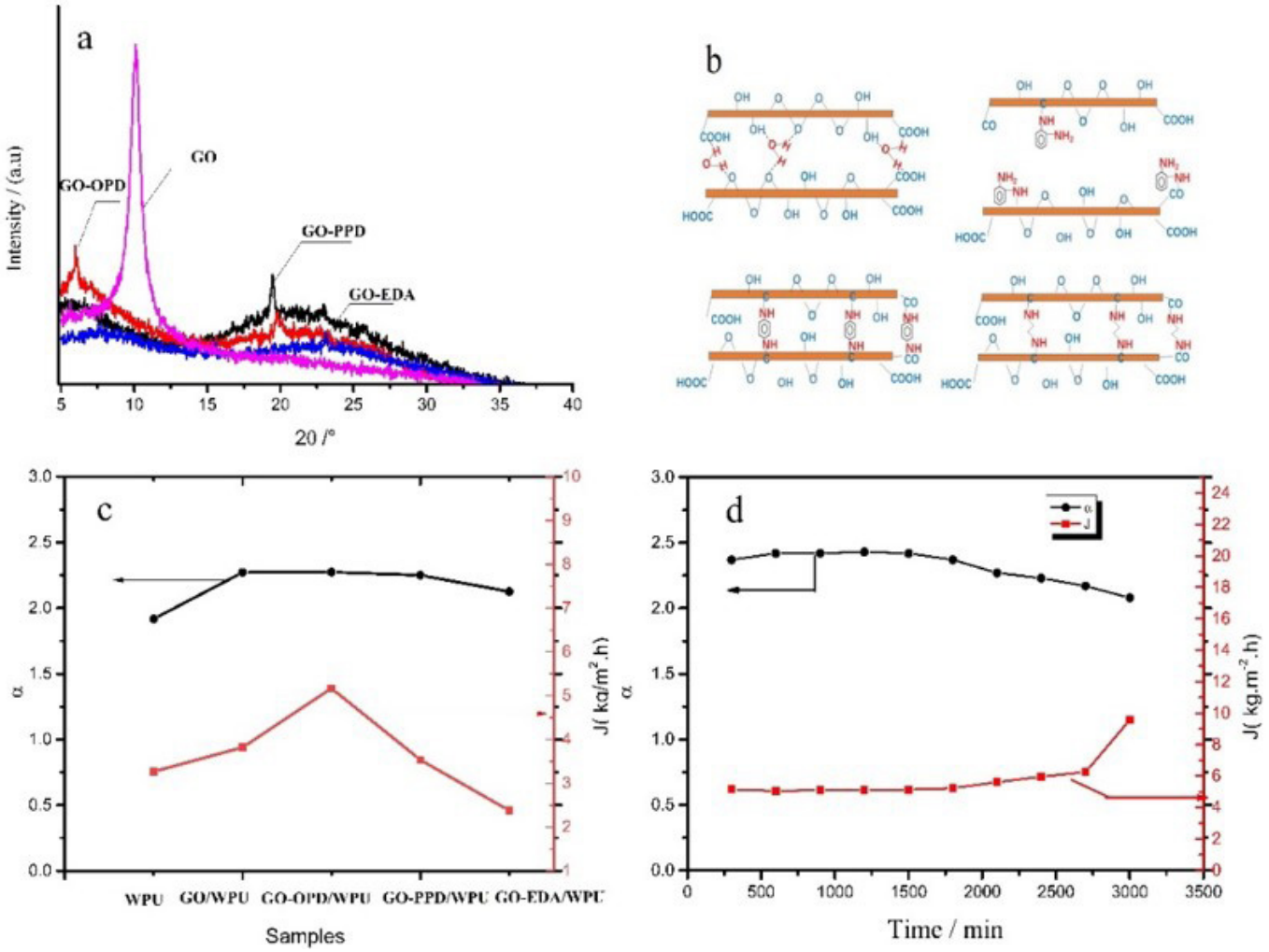

Figure 6. Pervaporation performance of rGO/WPU membranes. a: XRD patterns showed different interlayer structure of GO. b: Cartoon picture showed different path of WPU membranes. c: Pervaporation test results of different membranes. d: Pervaporation performance-time of GO-OPD/WPU membrane.

molecules are replaced by reducing agent, vertical cross-linking structure were build-up. Due to the aliphatic amino group consuming more oxygen-containing functional groups than aromatic amino does, the strong reducing activity of EDA make GO-EDA layers stacked together like a graphitized agglomeration structure. For PPD, it has a symmetrical structure and easily to form vertical cross-links to expand space, but the para-amino group is more active than the ortho-amino group, which will consume more oxygen-containing functional groups than that of OPD. So, GO-PPD showed a smaller interlayer distance than that of GO-OPD. Accordingly, in GO-OPD/WPU samples, due to the mild reducing activity, enough oxygen-containing functional groups remained to resists the accumulation of interlayers, and expanded GO-OPD interlayer distance, which was consistent with the XRD result.

Pervaporation (PV) test were carried out to investigate the separation performance of different membranes, and the results were shown in Figure 6c. Compared with the unmodified WPU membrane, the permeation flux J of all the modified WPU membrane changed significantly, but the separation factor α was few increased. It could be seen that GO-OPD / WPU showed superiorly PV separation performance [J = 5166.7 g/(m².h)], which was higher than GO-WPU [J = 3534.4 g / (m².h)], even 1.58 times of the unmodified WPU membrane [J = 3268.3 g/(m².h)]. The PV test results furtherly confirmed more spacing between GO-OPD/WPU membrane than the other GO/WPU, WPU and GO-EDA/ WPU membrane.

The stability of GO-OPD / WPU membrane was investigated by the continuous pervaporation experiment at 50 °C and under -0.1009 MPa osmotic pressure for 3000 minutes. As shown in Figure 6d, GO-OPD / WPU membrane maintained stable PV performance during continuous 2700 min experiments, indicating that GO-OPD / WPU still maintained membrane integrity for a long-time at the pervaporation press. 3000 minutes later, the value of J increased dramatically and α decreased significantly. This may be caused by the material excessively liquid swelling in the membrane, leading to the destruction of the hydrogen bonds between OPD-GO and WPU, thus more benzene and

cyclohexane passed through the gap between them, also known as "short circuit" phenomenon of the transmission channel. At this point, the membrane loses its sieving effect.

Packaging materials toxicity level should be as low as possible, which are important factors for the quality of products (Akarca, 2020), such as fruit preservation (Susilo et al., 2022), tuber crop (Pereira et al., 2021), meat (Qiao et al., 2022). Therefore, efforts should be made to build a bridge between GO/WPU membranes to conquer the cross-cutting effect of the two-dimensional structure in the next step. In this way, it will bring out good enough biocompatibility, providing a natural, d biodegradable, eco-friendly, intelligent, and sustainable polymer to the separation process.

Due to environmentally technological process, rGO / WPU may be a suitable packaging material with outstanding storage quality. The rGO endowed WPU membrane good mechanical properties, availing the food against physical harm. Hard-soft adjustable segment structure of WPU could be an excellent way to the control of food storage condition. Moreover, pervaporation, as one of highly efficient and economic membrane separation methods, is capable of separating aromatic compounds in raw material and eliminating baneful influence on the ecological environment. Thus rGO / WPU could be developed market need packing materials in many foods' storage in pristine condition for longer periods of time.

4 Conclusions

In our result, it was demonstrated that the improving pervaporation separation properties of benzene / cyclohexane have be gained by the modified GO-OPD/WPU membrane. All the rGO / WPU pervaporation membrane are prepared at low-temperature in situ generation method, without undergoing a complicated functionalization process. GO or rGO were physically co-extended with WPU through hydrogen bonding. It was demonstrated o-phenylenediamine with mild reducing ability, showed a superior interlayer expansion capability to other reducing agents. GO-OPD also played a role in the pervaporation performance of the WPU membrane. Even in trace doping amounts (0.03%) of GO-OPD, the flux of GO-OPD/WPU was 1.58 times that of WPU and GO/WPU, and still maintains good stability the pervaporation process for 2700 minutes.

Conflict of interest

There is no declaim.

Acknowledgements

This work was supported by the Natural Science Research Project of Anhui Educational Committee (KJ2021A1263), the Youth Talent Cultivation Project of North Minzu University (2021KYQD27, FWNX14), and the Key Research and Development Projects in Ningxia Province (2021BEF02013).

References

Akarca, G. (2020). Lipolysis and aroma occurrence in Erzincan Tulum cheese, which is produced by adding probiotic bacteria and ripened in various packages. *Food Science and Technology (Campinas)*, 40(1), 102-106. http://dx.doi.org/10.1590/fst.33818.

Akram, N., Saeed, M., & Usman, M. (2022). Role of macrodio1s in the synthesis and then no mechanica1 behavior of anti tack water bome po1yurethane dispersions. *Polymers*, 14(3), 572. http://dx.doi.org/10.3390/polym14030572. PMid:35160561.

Alshamkhani, M. T., Lahijani, P., Lee, K. T., & Mohamed, A. R. (2022). Electrochemical exfoliation of graphene using dual graphite electrodes by switching voltage and green molten salt electrolyte. *Ceramics International*, 48(15), 22534-22546. http://dx.doi.org/10.1016/j.ceramint.2022.04.268.

Burshtein, T. Y., Tamakuwala, K., Sananis, M., Grinberg, I., Samala, N. R., & Eisenberg, D. (2022). Understanding hydrazine oxidation electrocatalysis on undoped carbon. *Physical Chemistry Chemical Physics*, 24(17), 9897-9903. http://dx.doi.org/10.1039/D2CP00213B. PMid:35416204.

Chen, W., Liu, P., Min, L., Zhou, Y., Liu, Y., Wang, Q., & Duan, W. (2018). Non-covalently functionalized graphene oxide-based coating to enhance thermal stability and flame retardancy of PVA film. *Nano-Micro Letters*, 10(3), 39. http://dx.doi.org/10.1007/s40820-018-0190-8. PMid:30393688.

Esmaeili-Faraj, S. H., Hassanzadeh, A., Shakeriankhoo, F., Hosseini, S., & Vaferi, B. (2021). Diesel fuel desulfurization by alumina/polymer nanocomposite membrane: Experimental analysis and modeling by the response surface methodology. *Chemical Engineering and Processing*, 164, 108396. http://dx.doi.org/10.1016/j.cep.2021.108396.

Jia, Z. Q., Wang, Y., Shi, W. X., & Wang, J. L. (2016). Diamines cross-linked graphene oxide free-standing membranes for ion dialysis separation. *Journal of Membrane Science*, 520, 139-144. http://dx.doi.org/10.1016/j.memsci.2016.07.042.

Joshi, D. J., Koduru, J. R., Malek, N. I., Hussain, C. M., & Kailasa, S. K. (2021). Surface modifications and analytical applications of graphene oxide: a review. *Trends in Analytical Chemistry*, 144, 116448. http://dx.doi.org/10.1016/j.trac.2021.116448.

Joshi, R. K., Carbone, P., Wang, F. C., Kravets, V. G., Su, Y., Grigorieva, I. V., Wu, H. A., Geim, A. K., & Nair, R. R. (2014). Precise and ultrafast molecular sieving through graphene oxide membranes. *Science*, 343(6172), 752-754. http://dx.doi.org/10.1126/science.1245711. PMid:24531966.

Kong, L., Chen, Q., Shen, X. P., Xu, Z. Y., Xu, C., Ji, Z. Y., & Zhu, J. (2018). MOF derived nitrogen-doped carbon polyhedrons decorated on graphitic carbon nitride sheets with enhanced electrochemical capacitive energy storage performance. *Electrochimica Acta*, 265, 651-661. http://dx.doi.org/10.1016/j.electacta.2018.01.146.

Lada, Z. G. (2022). The investigation of spin-crossover systems by raman spectroscopy: a review. *Magnetochemistry (Basel, Switzerland)*, 8(9), 108. http://dx.doi.org/10.3390/magnetochemistry8090108.

Liu, L. X., Lu, J. Y., Zhang, Y., Liang, H. Y., Liang, D. S., Jiang, J. Z., Lu, Q. M., Quirino, R. L., & Zhang, C. Q. (2019). Thermosetting polyurethanes prepared with the aid of a fully bio-based emulsifier with high bio-content, high solid content, and superior mechanical properties. *Green Chemistry*, 21(3), 526-537. http://dx.doi.org/10.1039/C8GC03560A.

Muller, C., Neves, L. E., Gomes, L., Guimaraes, M., & Ghesti, G. (2020). Processes for alcohol-free beer production: a review. *Food Science and Technology (Campinas)*, 40(2), 273-28. http://dx.doi.org/10.1590/fst.32318.

Nairat, N., Hamed, O., Berisha, A., Jodeh, S., Algarra, M., Azzaoui, K., Dagdag, O., & Samhan, S. (2022). Cellulose polymers with β-amino ester pendant group: design, synthesis, molecular docking and application in adsorption of toxic metals from wastewater. *BMC*

Chemistry, 16(1), 43. http://dx.doi.org/10.1186/s13065-022-00837-7. PMid:35689266.

Panda, P. K., Sadeghi, K., & Seo, J. (2022). Recent advances in poly (vinyl alcohol)/natural polymer based films for food packaging applications: a review. *Food Packaging and Shelf Life*, 33, 100904. http://dx.doi.org/10.1016/j.fpsl.2022.100904.

Peng, L., Xu, Z., Liu, Z., Guo, Y., Li, P., & Gao, C. (2017). Ultrahigh thermal conductive yet superflexible graphene films. *Advanced Materials*, 29(27), 1700589. http://dx.doi.org/10.1002/adma.201700589. PMid:28498620.

Pereira, A. M., Petrucci, K. P. D. S., Gomes, M. D., Goncalves, D. N., Cruz, R. R. P., Ribeiro, F. C. S., & Finger, F. L. (2021). Quality of potato CV innovator submitted refrigeration and recondition. *Food Science and Technology (Campinas)*, 41(1), 30-48. http://dx.doi.org/10.1590/fst.26619.

Pramoda, K., Gupta, U., Chhetri, M., Bandyopadhyay, A., Pati, S. K., & Rao, C. (2017). Nanocomposites of c3n4 with layers of mos2 and nitrogenated rgo, obtained by covalent cross-linking: synthesis, characterization, and her activity. *ACS Applied Materials & Interfaces*, 9(12), 10664-10672. http://dx.doi.org/10.1021/acsami.7b00085. PMid:28267317.

Qian, Y. L., Zhou, C., & Huang, A. S. (2018). Cross-linking modification with diamine monomers to enhance desalination performance of graphene oxide membranes. *Carbon*, 136, 28-37. http://dx.doi.org/10.1016/j.carbon.2018.04.062.

Qiao, Z. H., Yin, M. Y., Qi, X. J., Li, Z. Z., Yu, Z., Chen, M., Xiao, T., & Wang, X. C. (2022). Freezing and storage on aquatic food: underlying mechanisms and implications on quality deterioration. *Food Science and Technology (Campinas)*, 42, e91322. http://dx.doi.org/10.1590/fst.91322.

Ramanavičius, S., Morkvėnaitė-Vilkončienė, I., Samukaitė-Bubnienė, U., Ratautaitė, V., Plikusienė, I., Viter, R., & Ramanavičius, A. (2022). Electrochemically deposite.molecularly imprinted polymer-based sensors. *Sensors (Basel)*, 22(3), 1282. http://dx.doi.org/10.3390/s22031282. PMid:35162027.

Rostovtseva, V., Faykov, I., & Pulyalina, A. (2022). A review of recent developments of pervaporation membranes for ethylene glycol purification. *Membranes*, 12(3), 312. http://dx.doi.org/10.3390/membranes12030312. PMid:35323787.

Sabry, N., Hussien, M. S. A., & Yahia, I. S. (2022). Eco-friendly synthesis of g-carbon nitride coated graphene nanocomposites for superior visible photodegradation of hydroquinone: physicochemical mechanisms and photo-fenton effect. *Journal of Photochemistry and Photobiology A Chemistry*, 426, 113734. http://dx.doi.org/10.1016/j.jphotochem.2021.113734.

Saini, P., Singh, M., Singh, S. P., & Mahapatro, A. K. (2018). Spectroscopic and electronic properties of polyallylamine functionalized graphene oxide films. *Vacuum*, 154, 110-114. http://dx.doi.org/10.1016/j.vacuum.2018.04.056.

Sang, L., Hao, W. T., Zhao, Y., Yao, L., & Cui, P. (2018). Highly aligned graphene oxide/waterborne polyurethane fabricated by in-situ polymerization at low temperature. *E-Polymers*, 18(1), 75-84. http://dx.doi.org/10.1515/epoly-2017-0141.

Shen, J., Chen, W., Lv, G., Yang, Z., Yan, J., Liu, X., & Dai, Z. (2021). Hydrolysis of nh3bh3 and nabh4 by graphene quantum dots-transition metal nanoparticles for highly effective hydrogen evolution. *International Journal of Hydrogen Energy*, 46(1), 796-805. http://dx.doi.org/10.1016/j.ijhydene.2020.09.153.

Sun, K., Wang, L., Wu, C., Deng, J. P., & Pan, K. (2017). Fabrication of α-Fe2O3@rGO/PAN nanofiber composite membrane for photocatalytic degradation of organic dyes. *Advanced Materials Interfaces*, 4(24), 1700845. http://dx.doi.org/10.1002/admi.201700845.

Susilo, B., Rohim, A., & Filayati, M. A. J. (2022). Vacuum drying as a natural preservation method of post-harvest lemon might accelerate drying duration and produce the high-quality of dried lemon slices. *Food Science and Technology (Campinas)*, 42, e58722.

Viveka, S. S., Logu, T., Ahsan, N., Asokan, K., Kalainathan, S., Sethuraman, K., & Okada, Y. (2022). Study of sub-band states formation in the optical band gap of cugas2 thin films by electronic excitations. *Journal of Physics and Chemistry of Solids*, 164, 110636. http://dx.doi.org/10.1016/j.jpcs.2022.110636.

Wang, B. C., Cao, Q., Shao, W., & Cui, Z. (2022a). Effects of vacancy defects on the interfacial thermal resistance of partially overlapped bilayer graphene. *Physical Chemistry Chemical Physics*, 24(9), 5546-5554. http://dx.doi.org/10.1039/D1CP03492H. PMid:35174847.

Wang, H., Liu, X., Yang, Z., He, H., Shao, X., & Bai, R. (2020). Preparation and characterization of hexamethylenediamine-modified graphene oxide/co-polyamide nanocomposites. *Polymers & Polymer Composites*, 28(6), 421-432. http://dx.doi.org/10.1177/0967391119887298.

Wang, S., Xu, L., & Wang, J. (2022b). Enhanced activation of peroxymonosulfate through exfoliated oxygen-doping graphitic carbon nitride for degradation of organic pollutants. *Chemical Engineering Journal*, 428, 131066. http://dx.doi.org/10.1016/j.cej.2021.131066.

Wu, W., Zhao, W., Gong, X., Sun, Q., Cao, X., Su, Y., Yu, B., Li, R. K. Y., & Vellaisamy, R. A. L. (2022). Surface decoration of halloysite nanotubes with poss for fire-safe thermoplastic polyurethane nanocomposites. *Journal of Materials Science and Technology*, 101(28), 107-117. http://dx.doi.org/10.1016/j.jmst.2021.05.060.

Wu, X., Xie, S., Xu, K., Huang, L., Wei, D., & Tian, J. (2021). Enhancing graphene retention and electrical conductivity of plasma-sprayed alumina/graphene nanoplatelets coating by powder heat treatment. *Coatings*, 11(6), 643. http://dx.doi.org/10.3390/coatings11060643.

Xu, W. L., Fang, C., Zhou, F., Song, Z. N., Liu, Q. L., Qiao, R., & Yu, M. (2017). Self-assembly: a facile way of forming ultrathin, high-performance graphene oxide membranes for water purification. *Nano Letters*, 17(5), 2928-2933. http://dx.doi.org/10.1021/acs.nanolett.7b00148. PMid:28388082.

Yang, G., Xie, Z., Cran, M., Wu, C., & Gray, S. (2020). Dimensional nanofillers in mixed matrix membranes for pervaporation separations: a review. *Membranes*, 10(9), 193. http://dx.doi.org/10.3390/membranes10090193. PMid:32825195.

Yang, J., Gong, D., Li, G., Zeng, G., Wang, Q., Zhang, Y., Liu, G., Wu, P., Vovk, E., Peng, Z., Zhou, X., Yang, Y., Liu, Z., & Sun, Y. (2018). Self-assembly of thiourea-crosslinked graphene oxide framework membranes toward separation of small molecules. *Advanced Materials*, 30(16), e1705775. http://dx.doi.org/10.1002/adma.201705775. PMid:29537669.